Preprints (www.preprints.org) | NOT PEER-REVIEWED | Posted: 11 July 2018 doi:10.20944/preprints201807.0205.v1

Epoxide Functional γ-Al_2O_3/Fe_3O_4/SiO_2 Ceramic Nanocomposite Particles as Adsorbent for Reactive Azo Dye: Understanding Surface Property

Sadia Salsabil Bristy[1], Mohammad Mostafizar Rahman[2], Mohammad Mahbubor Rahman[1], Mohammad Ashraful Alam[1], Mohammad Rabiul Karim[1] and Hasan Ahmad[1,*]

[1] Department of Chemistry, Rajshahi University, Rajshahi 6205, Bangladesh

[2] Berger Paints Bangladesh Ltd., Dhaka Factory, Nabinagar, Savar, Dhaka 1340, Bangladesh

∗Correspondence: hahmad@ru.ac.bd; Tel: +88-0721-711107

ORCID

Hasan Ahmad: 0000-0003-1499-167X

© 2018 by the author(s). Distributed under a Creative Commons CC BY license.

Preprints (www.preprints.org) | NOT PEER-REVIEWED | Posted: 11 July 2018 doi:10.20944/preprints201807.0205.v1

Abstract: In this investigation magnetic γ-Al_2O_3 ceramic nanocomposite particles bearing epoxide functionality are prepared following a multistep process. The ultimate nanocomposite particles are named as γ-Al_2O_3/Fe_3O_4/SiO_2/poly(glycidyl methacrylate (PGMA). The surface property is evaluated by carrying out the adsorption study of Remazol navy (RN), a model reactive azo dye, on both γ-Al_2O_3/Fe_3O_4/SiO_2 and γ-Al_2O_3/Fe_3O_4/SiO_2/PGMA nanocomposite particles. The adsorption is carried out at the point of zero charge (PZC) to neutralize the effect of particle surface charge. The adsorption rate is very fast, reached equilibrium (q_e) value within five min. Due to mesoporous structure of silica layer γ-Al_2O_3/Fe_3O_4/SiO_2 nanocomposite particles possessed relatively higher specific surface area and magnitude of adsorption is dependent on the total specific surface area. The introduction of epoxide functionality favored high adsorption capacity in mass per unit surface area. The adsorption process strictly followed Langmuir model. Thermodynamic equilibrium parameters implied that irrespective of surface functionality the adsorption process is spontaneous and exothermic. Pseudo-second-order rate kinetic model is more appropriate to explain the adsorption kinetics.

Keywords: γ-alumina; nanocomposite particle; epoxide functionality; adsorption; Remazol navy.

Preprints (www.preprints.org) | NOT PEER-REVIEWED | Posted: 11 July 2018 doi:10.20944/preprints201807.0205.v1

1. Introduction

Alumina (Al_2O_3) nanocrystals constitutes important class of nanoscale ceramic materials, possess desirable surface properties such as high surface area, thermal, mechanical and chemical stability, Lewis acid property and porosity [1-5]. These properties make them useful in high-temperature catalyst or catalytic support, tissue scaffolds, coating formulation, composite reinforcing materials, sorbent and membrane [6-16]. Recently researchers are continuously thriving for new class of composite materials to widen the application potential as well as to overcome the limitations such as tendency to aggregation, poor functionality and poor compatibility with the aqueous environment generally observed for metal oxides. However, only few research articles are available on the preparation of inorganic-organic hybrid composite materials from Al_2O_3 nanoparticles. Khabibullin *et al*. grafted poly(methyl methacrylate) brushes on α-Al_2O_3 nanoparticles via surface initiated atom transfer radical polymerization [7]. Popat *et al.* designed poly(ethylene glycol) (PEG) surface modified Al_2O_3 composite particles for targeted drug delivery system [8]. The porous surface of Al_2O_3 was first hydroxylated and finally reacted with silane coupled PEG. Jackson *et al.* modified 10 μm sized Al_2O_3 particles with epoxy monolayer via self-assembly and curing of epoxy fluids [9]. In another similar work ultrathin polypyrrole film was developed on Al_2O_3 particles using hexanoic acid as a template [10]. In a recently published article Anaya *et al.* modified the surface of γ-Al_2O_3 particles with stearic, palmitic, erucic and oleic acids and finally prepared high performance biocompatible polysulfone/ γ-Al_2O_3 nanocomposite simply via self-assembly through cooling process [11].

In a recently published article Bristy *et al.* optimized the preparation conditions of epoxide polymer layered magnetic γ-Al_2O_3 nanocomposite particles named as γ-Al_2O_3/Fe_3O_4/SiO_2/poly(glycidyl methacrylate (PGMA) [17]. The preparation scheme of

Preprints (www.preprints.org) | NOT PEER-REVIEWED | Posted: 11 July 2018 doi:10.20944/preprints201807.0205.v1

nanocomposite particles is shown in Figure 1. γ-Al_2O_3 core particles were prepared by sol-gel technique and then doped with Fe_3O_4 nanoparticles. To improve the compatibility before next step seeded polymerization with GMA magnetic γ-Al_2O_3 particles were modified with mesoporous SiO_2 layer. Size distribution, morphology, surface composition and magnetic property of nanocomposite particles were analyzed. In this investigation the surface property of γ-Al_2O_3/Fe_3O_4/SiO_2/PGMA nanocomposite particles was evaluated by carrying out adsorption of Remazol navy (RN), a model reactive azo dye. RN is a widely used textile dye in the subcontinent. The leakage of dye containing wastewater into the environment is known to possess serious health hazards. The discharged dye molecules in water remains for long time because they are naturally non-degradable and most of them are strongly poisonous and proven to be carcinogenic [18-24]. The removal of dye from water bodies is therefore indispensible. Adsorption is an important technique for removing dye because it is easy to operate and also possible to reuse both dye and adsorbent. Here the adsorption behavior of RN on γ-Al_2O_3/Fe_3O_4/SiO_2/PGMA nanocomposite particles was compared with that on γ-Al_2O_3/Fe_3O_4/SiO_2 nanocomposite particles as reference material. The inclusion of epoxide functionality on γ-Al_2O_3 particles is expected to improve several properties like hydrophilicity, colloidal stability and reactivity with sensitive compounds like reactive dyes, diamines and fluorescent compounds [25-27]. Magnetic nature would favor easy separation of adsorbent from the medium by applying magnetic field. It can be mentioned that only few number of adsorption studies are available with remazol group dyes (such as remazol brilliant blue, remazol red, remazol black b, remazol brilliant violet) on natural activated carbon and the adsorption process was found to be relatively slow, taken several hours for maximum adsorption [28-30].

Preprints (www.preprints.org) | NOT PEER-REVIEWED | Posted: 11 July 2018 doi:10.20944/preprints201807.0205.v1

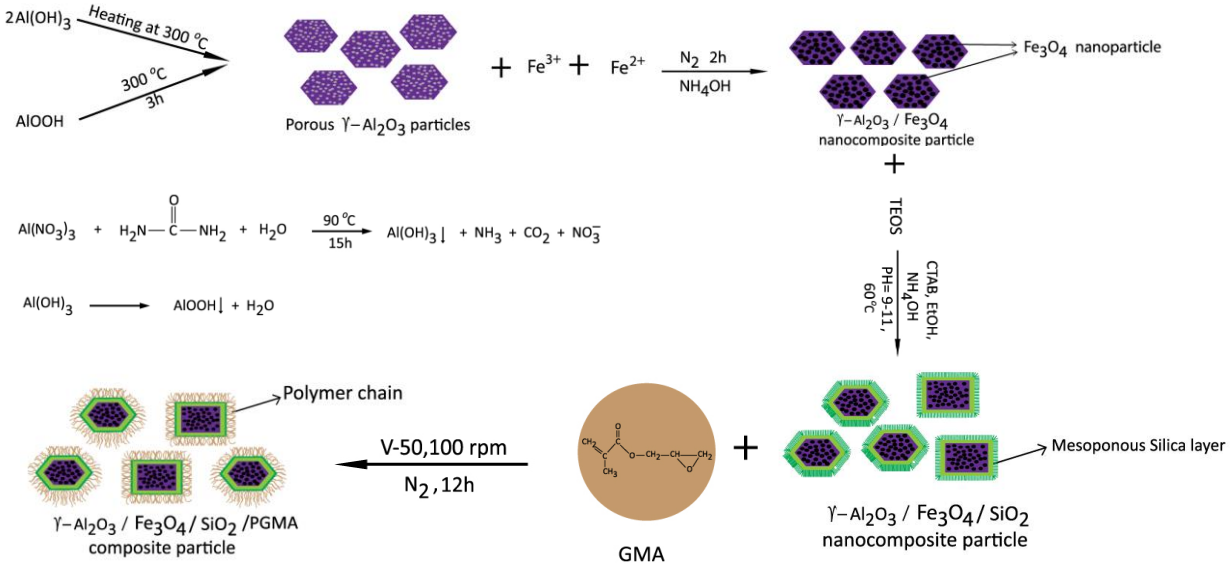

Figure 1. Preparation of γ-Al_2O_3/Fe_3O_4/SiO_2/PGMA ceramic nanocomposite particles.

2. Materials and Methods

2.1. Chemicals and Instruments

Monomer grade GMA from Fluka, Chemika, Switzerland was purified to remove inhibitors by passing through activated basic alumina column. Tetraethyl orthosilicate (TEOS) from Sigma-Aldrich Chemie GmbH, USA, aluminium nitrate nonahydrate ($Al(NO_3)_3$,$9H_2O$) and urea both from E-Merck, Germany, sodium dodecyl sulphate (SDS), cetyl trimethyl ammonium bromide (CTAB) both from Fluka, Biochemica, Switzerland were used as received. 2,2'-Azobis(2-amidinopropane)dihydrochloride (V-50) from LOBA Chem. India, was recrystallized from distilled water before use. RN was obtained from Dystar India Pvt. Ltd., Mumbai and used as received. Ferric chloride ($FeCl_3$), ferrous sulphate heptahydrate ($FeSO_4.7H_2O$), NH_4OH, citric acid, HNO_3 and other chemicals were of either analytical or reagent grade. Deionized water and ethanol were distilled using a glass (pyrex) distillation apparatus.

Preprints (www.preprints.org) | NOT PEER-REVIEWED | Posted: 11 July 2018 doi:10.20944/preprints201807.0205.v1

Transmission electron microscope or TEM (Zeiss EM-912, Omega) was used to see the morphology and particle size distribution. FTIR (Perkin Elmer, FTIR-100, UK), and X-ray photoelectron spectroscopy, XPS (PHI X-tool, ULVAC-PHI, Japan) were used to confirm the surface structural composition. Vibrating sample magnetometer, VSM (MicroSense, EV9, USA) was used for the measurement of magnetic property.

2.2. Preparation of Reference Fe_3O_4 Nanoparticles

Reference Fe_3O_4 nanoparticles were prepared by co-precipitation of Fe^{2+} and Fe^{3+} from their aqueous 25% NH_4OH solutions (molar ratio 1:1.87) in a three necked round flask. The co-precipitation was carried out in a nitrogen atmosphere for 2 h at 85°C. The prepared Fe_3O_4 emulsion was treated with HNO_3 (2M) for 15 min, washed with water to neutral pH and finally stabilized by slowly adding citric acid (40 g). Before characterization Fe_3O_4 nanoparticles were washed magnetically by repeated sedimentation to remove free citric acid.

2.3. Preparation of γ-Al_2O_3/Fe_3O_4/SiO_2/PGMA Nanocomposite Particles

γ-Al_2O_3/Fe_3O_4/SiO_2/PGMA nanocomposite particles were prepared following a multistep process. In the first step γ-Al_2O_3 particles were prepared from $Al(NO_3)_3$,$9H_2O$ (35 g) and urea (72 g) maintaining the molar ratio of Al^{3+}/urea at 1/13. The aluminium-urea saturated solution was heated in a three necked round bottomed flask immersed in thermostat oil bath maintained at 90 °C for 12 h. With the progress of the reaction the pH gradually increased from ~ 2 to ~6. The Al_2O_3 sol produced was heated for another 3 h to a transparent gel. The Al_2O_3 gel was finally dried at 300 °C for 3 h in presence of air to produce amorphous γ-Al_2O_3 powder.

Preprints (www.preprints.org) | NOT PEER-REVIEWED | Posted: 11 July 2018 doi:10.20944/preprints201807.0205.v1

γ-Al_2O_3 particles were doped with Fe_3O_4 nanoparticles to produce γ-Al_2O_3/Fe_3O_4 nanocomposite particles. For this, in-situ co-precipitation of Fe^{2+} (0.3753 g) and Fe^{3+} (0.438 g) from their alkali solution (25% NH_4OH) was carried out in presence of cationic CTAB (0.0125 g) stabilized γ-Al_2O_3 (0.5 g) particles. The yield of reference Fe_3O_4 nanoparticles was considered to fix the weight ratio of alumina/magnetite at 1/2. Before repeated washing the prepared black colored γ-Al_2O_3/Fe_3O_4 nanocomposite dispersion was treated with 2 M HNO_3 (1.3 g) for 15 min. γ-Al_2O_3/Fe_3O_4 nanocomposite particles were stabilized before next step modification by adding 0.4 M citric acid and washed again repeatedly by magnetic separation and redispersion in distilled deionized water.

The surface modification of γ-Al_2O_3/Fe_3O_4 nanocomposite particles by mesoporous silica (SiO_2) layer was carried out following a slightly changed process as available in literature [31,32]. Deionized water (24 g), ethanol (4 g) and mesoporous template, CTAB (0.196 g) taken in a three necked round flask were mixed thoroughly at 60 °C. After the complete solubilization of CTAB, γ-Al_2O_3/Fe_3O_4 nanocomposite particles (0.5 g) were added to the mixture. Then pH of the mixture was adjusted at 9-11 using 25% NH_3 solution (0.26 g), a favorable condition for the formation of SiO_2 layer. Finally TEOS (0.5 g) was added dropwise and the reaction was continued for 2 h at 60 °C. The formation of γ-Al_2O_3/Fe_3O_4/SiO_2 nanocomposite particles was confirmed as the black solution gradually turned fade. The nanocomposite dispersion was subjected to repeated washing (initially by ethanol and finally by deionized water) with five cycles of magnetic separation.

Finally γ-Al_2O_3/Fe_3O_4/SiO_2/PGMA nanocomposite particles were prepared by seeded polymerization of GMA (0.4 g) in presence of γ-Al_2O_3/Fe_3O_4/SiO_2 nanocomposite particles (0.2 g) and distilled water (60.0 g). The polymerization was initiated at 75 °C by adding aqueous

Preprints (www.preprints.org) | NOT PEER-REVIEWED | Posted: 11 July 2018 doi:10.20944/preprints201807.0205.v1

solution of V-50 (0.012 g) initiator and the reaction was continued for 12 h under a nitrogen atmosphere.

2.4. Characterization

For TEM observation a drop of diluted sample (0.01% solid) was placed on the carbon-coated copper grid, dried at room temperature and then observed at an accelerating voltage of 100 kV. BET method was used to measure the specific surface areas (S_{BET}) of the powdered nanocomposite particles at 77 K with NOVA3000e apparatus. Prior to the measurement the sample was dried in oven at 70 °C. The surface elemental composition of nanocomposite particles dried onto a carbon tape was evaluated by XPS. This was equipped with a monochromatic Al Ka radiation (1486.6eV) at 104 W and 20 kV and an X-ray current of 20 (micro)A. The pressure in the measurement chamber was ca. 8.0 10^{-7} Pa. The step size was 0.25eV for the both survey and high resolution spectra (pass energy 280eV).

2.5. Point of Zero Charge (PZC) of Nanocomposite Particles

The PZC of each of the γ-Al_2O_3/Fe_3O_4/SiO_2 and γ-Al_2O_3/Fe_3O_4/SiO_2/PGMA nanocomposite particles was determined by using salt addition method. 20 mL of 0.1 M $NaNO_3$ solution and 0.05 g of nanocomposite particles were mixed in a 100 mL beaker. The pH value was adjusted to 5, 6, 7, 8, and 9 respectively using either of the diluted NaOH or HNO_3 solution. The mixture was then magnetically stirred at 25 ^oC for 24 h. The change in pH value, ΔpH, (difference between initial and final pH) was plotted against initial pH value. The pH at which ΔpH is zero was taken as the PZC of nanocomposite particles.

Preprints (www.preprints.org) | NOT PEER-REVIEWED | Posted: 11 July 2018 doi:10.20944/preprints201807.0205.v1

2.6. Adsorption of RN on Nanocomposite Particles

30 mL of RN (100 mg L^{-1}) aqueous solution was mixed with 0.01 g of γ-$Al_2O_3/Fe_3O_4/SiO_2$/PGMA nanocomposite particles and the pH value was immediately adjusted to the PZC (pH 7.45). The nanocomposite-dye mixture was magnetically stirred at 303 K for different time intervals to optimize the equilibrium adsorption time. After each specific time interval γ-$Al_2O_3/Fe_3O_4/SiO_2$/PGMA nanocomposite particles were magnetically separated and finally centrifuged at 12000 rpm. Two-step separation was carried out to avoid the presence of dirt particles. The magnitude of dye adsorption was then estimated by measuring the absorbance of the supernatant using a UV-visible spectrophotometer at the λ_{max} of 620 nm. Initial dye concentration and calibration curve were used for this purpose.

For comparative study adsorption on γ-$Al_2O_3/Fe_3O_4/SiO_2$ nanocomposite particles was also carried out under the same conditions at pH 7.20 corresponding to the PZC.

Dye uptake at equilibrium, q_e (mg g^{-1}), was determined by

$$q_e = (C_o - C_e)V/W \quad \text{---------- (1)}$$

where C_o and C_e (mg L^{-1}) are the initial and equilibrium concentrations of the dye solutions, V (L) is volume of the solution, and W (g) is the mass of nanocomposite particles taken as adsorbent.

Dye adsorption efficiency (%) was calculated by using following expression:

$$\% R = [(C_o - C_e)/C_o] \times 100 \quad \text{---------- (2)}$$

The effect of adsorbent dose was studied by mixing variable amounts of each γ-$Al_2O_3/Fe_3O_4/SiO_2$/PGMA and γ-$Al_2O_3/Fe_3O_4/SiO_2$ nanocomposite particles with 30 mL of 100 mg L^{-1} RN aqueous solution, pH was adjusted to the PZC and equilibrated for 5 min (optimized from the previous experiment) at 303 K to achieve the maximum adsorption.

Preprints (www.preprints.org) | NOT PEER-REVIEWED | Posted: 11 July 2018 doi:10.20944/preprints201807.0205.v1

The equilibrium adsorption experiments were conducted as continuous experiment under identical conditions with variable initial RN concentrations (20, 40, and 45 mg g^{-1}) and temperatures (283, 303, and 323 K) using fixed amount (0.01 g) of $Al_2O_3/Fe_3O_4/SiO_2$/PGMA nanocomposite particles. Whereas for γ-$Al_2O_3/Fe_3O_4/SiO_2$ nanocomposite particles RN initial concentrations were varied between 40 to 60 mg g^{-1}. Langmuir, Freundlich and Temkin adsorption isotherms were used to describe the adsorption behavior.

Langmuir isotherm [33] a theoretical model valid for monolayer adsorption is expressed by the following nonlinear equation:

$$q_e = q_{max} \cdot b \cdot C_e / (1 + b \cdot C_e) \quad \text{----------} \quad (3)$$

where, q_e (mg g^{-1}) is the amount of dye adsorbed per unit mass of the nanocomposite particles at equilibrium, C_e (mg L^{-1}) is the equilibrium concentration of dye left out in the supernatant, q_{max} (mg g^{-1}) is the theoretical monolayer adsorption capacity and b (L mg^{-1}) is the Langmuir constant depicting the energy and affinity of adsorption.

The linear equation of Freundlich adsorption isotherm model [34] on heterogeneous surface can be expressed as:

$$\ln q_e = \ln K_f + 1/n \ln C_e \quad \text{----------} \quad (4)$$

where K_f (mg g^{-1}) is a constant relating to the adsorption capacity and n (g L^{-1}) is an empirical parameter measuring the adsorption intensity.

The linear form of Temkin adsorption isotherm model [35] suitable for explaining the chemisorption adsorption mechanism is given below:

$$q_e = B. \ln A_T + B. \ln C_e \quad \text{----------} \quad (5)$$

where B (= RT/b) is Temkin constant representing the heat of adsorption, R is universal gas constant (8.314 J/mol·K), T is the absolute temperature (K), A_T (L mg^{-1}) is the equilibrium

Preprints (www.preprints.org) | NOT PEER-REVIEWED | Posted: 11 July 2018 doi:10.20944/preprints201807.0205.v1

binding constant relating to maximum binding energy. The constants A_T and B were determined by plotting q_e vs ln C_e.

To understand the nature of interaction thermodynamic parameters such as changes in free energy, enthalpy and entropy (ΔG, ΔH and ΔS) were also explored using the following equations:

$$\ln K_c = \Delta S/R - \Delta H/RT \quad \text{---------- (6)}$$

$$\Delta G = \Delta H - T\Delta S \quad \text{---------- (7)}$$

Where, K_C is the thermodynamic equilibrium constant.

2.7. Reuse of γ-Al_2O_3/Fe_3O_4/SiO_2/PGMA Nanocomposite Particles

A desorption experiment was performed to investigate the reusability of the nanocomposite particles as adsorbent. The adsorption/recycle experiment on γ-Al_2O_3/Fe_3O_4/SiO_2/PGMA nanocomposite particles was started with 0.035 g nanocomposite particles and 50 mg L^{-1} RN aqueous solution (30 mL). After each successive adsorption at 303 K the dye loaded adsorbent was treated with 30 mL 1 M NaOH solution for 24 h at 50 °C. Then nanocomposite particles were magnetically recovered, washed repeatedly (5 times) with distilled deionized water before studying the adsorption again. Similar adsorption/recycle measurement was also carried out with γ-Al_2O_3/Fe_3O_4/SiO_2 nanocomposite particles using 30 mL of 100 mg L^{-1} dye solution.

3. Results and Discussion

3.1. Characterization of Nanocomposite Particles

TEM images of γ-Al_2O_3 particles and corresponding nanocomposite particles are illustrated in Figure 2. The particles were all washed by repeated replacement of continuous phase with

Preprints (www.preprints.org) | NOT PEER-REVIEWED | Posted: 11 July 2018 doi:10.20944/preprints201807.0205.v1

fresh distilled water before characterization. γ-Al_2O_3 particles possessed some interesting hexagonal flake shaped morphology. The size is ranged between 100 to 400 nm. The formation of spherical, cubic as well as tetragonal shaped particles is also possible as the image shows only a portion of the sample. The difference in contrast between dark and light parts in the magnified inset image is attributed to the porous γ-Al_2O_3 particles. After magnetization the morphology of γ-Al_2O_3/Fe_3O_4 nanocomposite particles (Figure 2b) changed a bit. The deposition of Fe_3O_4 nanoparticles increased the contrast of γ-Al_2O_3 particles. Fe_3O_4 nanoparticles are arranged into needle like fashion and grown from the surface of γ-Al_2O_3 particles. As the γ-Al_2O_3/Fe_3O_4 nanocomposite particles were magnetically washed prior to the TEM observation some free needle like Fe_3O_4 nanoparticles might also be present. TEM image of γ-Al_2O_3/Fe_3O_4 nanocomposite particles supported the assumption made regarding the formation of rectangular shaped γ-Al_2O_3 particles along with hexagonal flake shaped particles. In order to improve the compatibility with organic PGMA the surface of γ-Al_2O_3/Fe_3O_4 nanocomposite particles was modified with mesoporous SiO_2 layer following treatment with TEOS [36]. The penetration of GMA monomer into the mesoporous SiO_2 channel may also favor seeded polymerization, hindering secondary nucleation. Both γ-Al_2O_3/Fe_3O_4/SiO_2 and γ-Al_2O_3/Fe_3O_4/SiO_2/PGMA nanocomposite particles almost retained the hairy needle like morphology of γ-Al_2O_3/Fe_3O_4. Relative to γ-Al_2O_3/Fe_3O_4/SiO_2 nanocomposite particles the average thickness of hairy structure increased by around 4 nm after seeded polymerization. Flake shaped γ-Al_2O_3/Fe_3O_4 nanocomposite particles with light as well as dark background overlapped with hairy structure is also visible in either case. These results suggested that the surface of γ-Al_2O_3 particles has ultimately been modified according to the reaction protocol (Figure 1). The specific surface area (S_{BET}) of γ-Al_2O_3/Fe_3O_4/SiO_2 nanocomposite particles (149.63 m^2 g^{-1}) is comparatively high

Preprints (www.preprints.org) | NOT PEER-REVIEWED | Posted: 11 July 2018 doi:10.20944/preprints201807.0205.v1

compared to γ-Al_2O_3/Fe_3O_4/SiO_2/PGMA nanocomposite particles (53.16 m^2 g^{-1}). This is possibly attributed to the reduction of surface porosity and increase in average size following seeded polymerization of GMA.

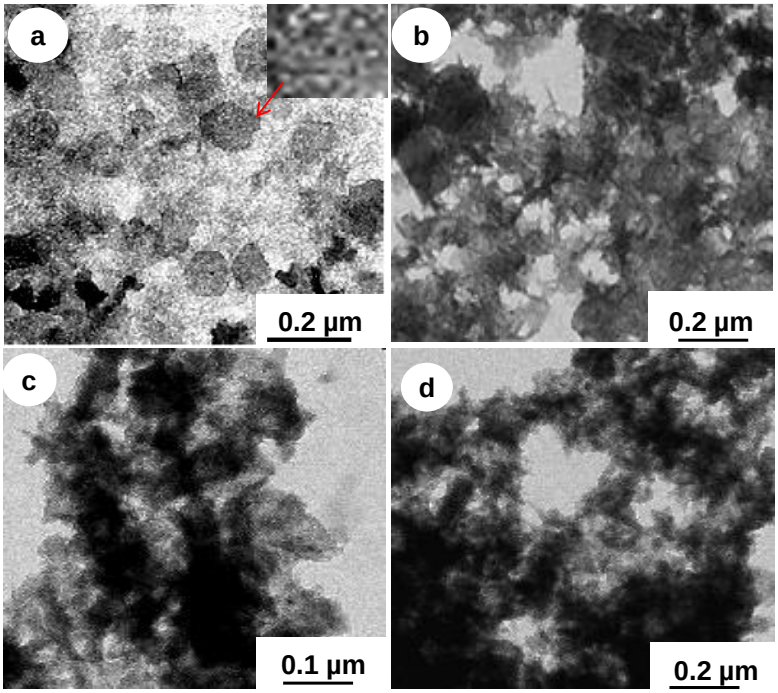

Figure 2. TEM photographs of (a) γ-Al_2O_3 particles, (b) γ-Al_2O_3/Fe_3O_4, (c) γ-Al_2O_3/Fe_3O_4/SiO_2, and (d) γ-Al_2O_3/Fe_3O_4/SiO_2//PGMA nanocomposite particles.

The surface composition of the particles was confirmed by XPS study**.** A comparative plot of XPS survey spectra for γ-Al_2O_3 particles, γ-Al_2O_3/Fe_3O_4, γ-Al_2O_3/Fe_3O_4/SiO_2 and γ-Al_2O_3/Fe_3O_4/SiO_2/PGMA nanocomposite particles is shown in Figure 3**.** The intensity of Al2p signal appeared at ~ 73 eV in γ-Al_2O_3 particles is gradually reduced after each step of surface modification. The signal intensity of Al2p is reduced to ca 1.5 atom% in γ-Al_2O_3/Fe_3O_4/SiO_2/PGMA nanocomposite particles from ca 10 atom% in γ-Al_2O_3 particles. The modification of γ-Al_2O_3/Fe_3O_4 nanocomposite particles by SiO_2-PGMA layer also decreased combined signal intensity of two characteristic doublets at 710.5 and 725.4 eV for $Fe2p_{3/2}$ and

Preprints (www.preprints.org) | NOT PEER-REVIEWED | Posted: 11 July 2018 doi:10.20944/preprints201807.0205.v1

Fe2p$_{1/2}$ from ca 9.6 atom% in γ-Al_2O_3/Fe_3O_4 nanocomposite particles to ca 0.8 atom% in γ-Al_2O_3/Fe_3O_4/SiO_2/PGMA nanocomposite particles. Similarly the signal intensity due to Si2p in γ-Al_2O_3/Fe_3O_4/SiO_2 nanocomposite particles is ca 16 atom% and decreased to ca 3 atom% after seeded polymerization with PGMA. All these results confirmed the surface modification of γ-Al_2O_3 particles successively by Fe_3O_4, SiO_2, and PGMA layers.

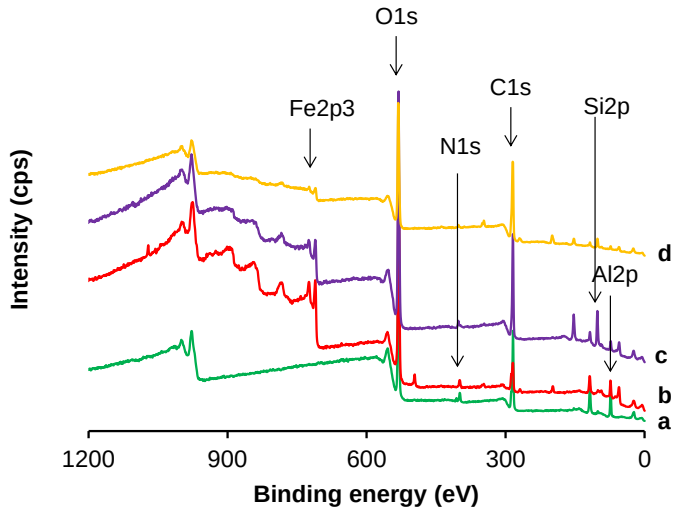

Fig. 3. XPS survey spectra of a) γ-Al_2O_3 particles, b) γ-Al_2O_3/Fe_3O_4, (c) γ-Al_2O_3/Fe_3O_4/SiO_2, and (g) γ-Al_2O_3/Fe_3O_4/SiO_2/PGMA nanocomposite particles.

The magnetization curves of magnetically separated γ-Al_2O_3/Fe_3O_4 and γ-Al_2O_3/Fe_3O_4/SiO_2/PGMA nanocomposite particles at room temperature up to a field of 20 kOe is shown in Figure 4. The saturation magnetization (M_s) decreased from an initial value of 14.0 emu/g for γ-Al_2O_3/Fe_3O_4 nanocomposite particles to 4.8 emu/g after modification with nonmagnetic SiO_2 and PGMA. The superparamagnetic nature can be confirmed from zero coercivity (H_c) or remnance in magnetization. The classic "S" shape magnetization curve also confirmed the superparamagnetic property. The nanocomposite particles would therefore be

Preprints (www.preprints.org) | NOT PEER-REVIEWED | Posted: 11 July 2018 doi:10.20944/preprints201807.0205.v1

quickly dispersed once the magnetic field is removed. It is also obvious that γ-Al_2O_3/Fe_3O_4/SiO_2/PGMA nanocomposite particles can be easily recycled after recovery from aqueous solution (inset of Figure 4). From the economic viewpoint magnetic separable property of nanocomposite particles would be important in water treatment application.

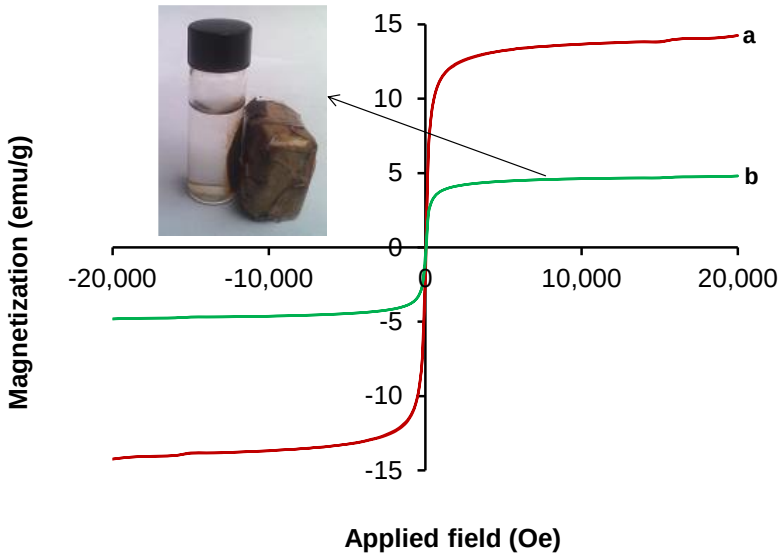

Figure 4. The hysteresis loops of magnetically separated a) γ-Al_2O_3/Fe_3O_4 and b) γ-Al_2O_3/Fe_3O_4/SiO_2/PGMA nanocomposite particles. Inset image shows the separation of γ-Al_2O_3/Fe_3O_4/SiO_2/PGMA nanocomposite particles in external magnetic field.

3.2. Adsorption Study of RN

One way of measuring the surface activity of nanocomposite particles is to study the adsorption behavior. RN a kind of reactive azo dye is known to possess different types of reactive groups along with azo-group and is capable of forming covalent bond with textile fibers such as cotton [37]. The use of azo dyes is posing serious threat as dye precursors or their biotransformation products are creating various toxicities like carcinogenic and mutagenic effects [38], teratogenicity in frog embryos [39], enzymic degradation metabolites toxicity [40],

Preprints (www.preprints.org) | NOT PEER-REVIEWED | Posted: 11 July 2018 doi:10.20944/preprints201807.0205.v1

and phytotoxicity [41]. The adsorption study was basically carried out on γ-$Al_2O_3/Fe_3O_4/SiO_2$/PGMA nanocomposite particles. To see any improvement in adsorption following epoxide functionalization a comparative adsorption study on γ-$Al_2O_3/Fe_3O_4/SiO_2$ nanocomposite particles was also carried out.

In order to avoid the ionic interaction, the adsorption of RN on nanocomposite particles was studied at the respective PZC which were found to be 7.20 and 7.45 for γ-$Al_2O_3/Fe_3O_4/SiO_2$ and γ-$Al_2O_3/Fe_3O_4/SiO_2$/PGMA nanocomposite particles respectively (Figure S1). PZC represents a state when the electric charge density of nanocomposite particles is zero. It is expected that ionization of sulfonic groups in RN at pH below the PZC would favor the adsorption on positively charged nanocomposite particles.

Figure 5 displays the effect of contact time on the adsorption of RN. It is observed that the adsorption of the dye is very rapid and reached equilibrium within 5 min on both γ-$Al_2O_3/Fe_3O_4/SiO_2$ and γ-$Al_2O_3/Fe_3O_4/SiO_2$/PGMA nanocomposite particles. Initially the rapid adsorption is associated with the availability of larger number of vacant active sites on adsorbent surface. It is reasonable to assume that after 5 min only few adsorption sites are available to accommodate additional dye molecules. In the following experiments the contact time was therefore adjusted to 5 min to attain maximum adsorption. The difference in adsorption magnitude of RN on two types of nanocomposite particles is typically attributed to the difference in surface properties and more importantly the total specific surface area. The total specific surface area of γ-$Al_2O_3/Fe_3O_4/SiO_2$/PGMA nanocomposite particles (53.16 $m^2\ g^{-1}$) was found to be much less than that of γ-$Al_2O_3/Fe_3O_4/SiO_2$ nanocomposite particles (149.63 $m^2\ g^{-1}$). So, adsorption capacity in mass per unit area (mg m^{-2}) would be more acceptable for comparing the adsorption performance.

Preprints (www.preprints.org) | NOT PEER-REVIEWED | Posted: 11 July 2018 doi:10.20944/preprints201807.0205.v1

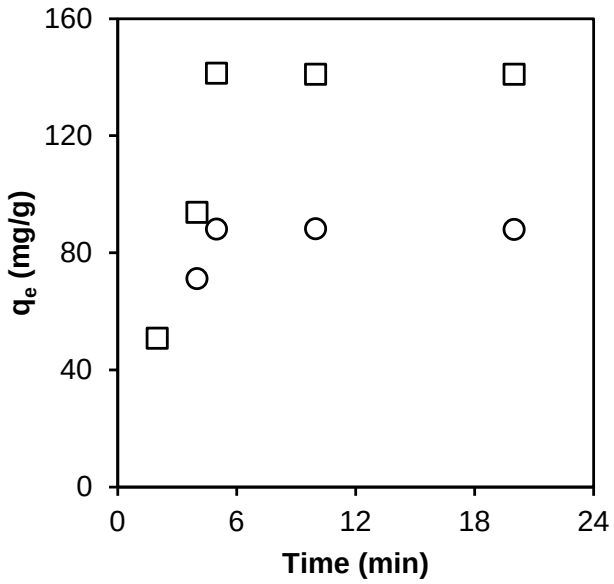

Figure 5. Contact time dependent change in adsorption amount of RN on γ-Al_2O_3/Fe_3O_4/SiO_2/PGMA (circle) and γ-Al_2O_3/Fe_3O_4/SiO_2 (square) nanocomposite particles at pH 7.45 and 7.20. Conditions: RN, 100 mg L^{-1}; Particles, 0.01 g; Total volume, 30 mL; Temperature, 303 K.

From an economical point of view it is important to know the minimum amount of nanocomposite particles (adsorbent dose) required for maximum adsorption. Figure 6 suggests that the adsorption efficiency increases with the increase in amount of nanocomposite particles. This behavior is ascribed to the increase in surface area with the increase in adsorbent dose. Initially the adsorption efficiency of RN on γ-Al_2O_3/Fe_3O_4/SiO_2/PGMA nanocomposite particles increases rapidly up to 0.03 g of nanocomposite particles and then slowed down to reach ~100% adsorption efficiency. Concurrently, with increasing adsorbent dose, the amount of adsorption decreases, thus causing a decrease in q_e value (Figure S2). Figure 6 indicates that the optimum adsorbent amount is 0.06 g to achieve ~100% adsorption efficiency but 0.01 g adsorbent is the

Preprints (www.preprints.org) | NOT PEER-REVIEWED | Posted: 11 July 2018 doi:10.20944/preprints201807.0205.v1

optimum amount for obtaining the maximum adsorption density. The reason may be that at lower adsorbent dose the dye molecules are more easily accessible. Therefore with increase in adsorbent dose there is less commensurate increase in adsorption leaving many adsorption sites unoccupied during adsorption [42,43]. Some authors also accounted for the interaction of nanocomposite particles at higher solid content causing partial overlapping or aggregation resulting in a decrease in effective adsorbent surface area [44]. Compared to this on γ-$Al_2O_3/Fe_3O_4/SiO_2$ nanocomposite particles the adsorption efficiency of RN reached ~100% rapidly at relatively low adsorbent content (0.03 g). The larger specific surface area of γ-$Al_2O_3/Fe_3O_4/SiO_2$ nanocomposite particles might have contributed to this adsorption behavior. The optimum amount of γ-$Al_2O_3/Fe_3O_4/SiO_2$ nanocomposite particles required for obtaining maximum adsorption density (Figure S2) remained as same (0.01 g) as epoxide functional nanocomposite particles.

Preprints (www.preprints.org) | NOT PEER-REVIEWED | Posted: 11 July 2018 doi:10.20944/preprints201807.0205.v1

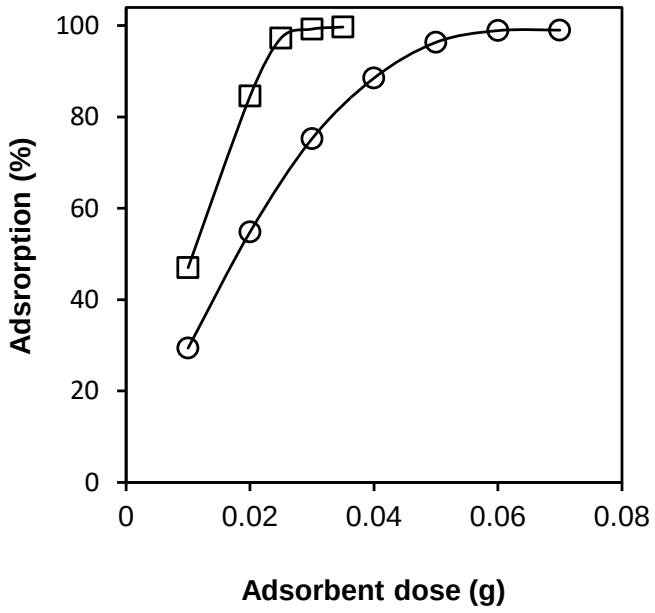

Figure 6. Dose dependent change in adsorption efficiency of RN on γ-Al_2O_3/Fe_3O_4/SiO_2/PGMA (circle) and γ-Al_2O_3/Fe_3O_4/SiO_2 (square) nanocomposite particles at pH 7.45 and 7.20. Conditions: RN, 100 mg L^{-1}; Total volume, 30 mL; Temperature, 303 K; Contact time, 5 min.

For γ-Al_2O_3/Fe_3O_4/SiO_2/PGMA nanocomposite particles the effect of initial RN dye concentration (C_0) on the equilibrium amount of adsorption (q_e) at different temperatures is shown in Figure 7A. This study was carried out to understand the effect of initial dye concentration and temperature on the amount of adsorption. The amount of adsorption at different temperatures increases with the increase of initial dye concentration. The increase of initial concentration acts as a driving force for the transfer of dye molecules from the aqueous solution to the surface of composite particles. Hence the interaction between dye molecules and particle surface increases at higher initial concentration. Figure 7A also suggests that amount of adsorption decreases with the increase of temperature hence the adsorption process is favorable at lower temperature. This decrease in the amount of adsorption with the increase in temperature

Preprints (www.preprints.org) | NOT PEER-REVIEWED | Posted: 11 July 2018 doi:10.20944/preprints201807.0205.v1

can be due to the increased solubility of dye molecules and dissociation of physical bonding (Van der Waals interaction) following increased entropy [45,46]. Comparatively the adsorption amount on γ-Al_2O_3/Fe_3O_4/SiO_2 nanocomposite particles (Figure 7B) dropped rapidly with increasing temperature. It is reasonable to assume that adsorption of RN on γ-Al_2O_3/Fe_3O_4/SiO_2 nanocomposite particles is mainly controlled by Van der Waals interaction whereas the adsorption on γ-Al_2O_3/Fe_3O_4/SiO_2/PGMA nanocomposite particles is controlled by both physical (Van der Waals interaction) and chemical bonding (hydrogen bonding and perhaps covalent linkage).

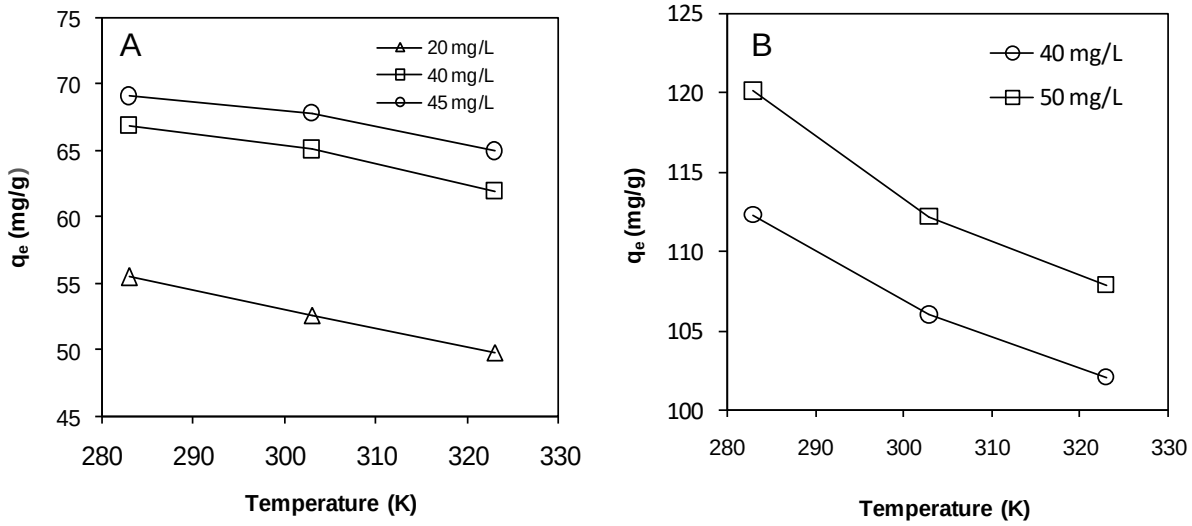

Figure 7. Initial RN concentration and temperature dependent adsorption behavior on A) γ-Al_2O_3/Fe_3O_4/SiO_2/PGMA, and B) γ-Al_2O_3/Fe_3O_4/SiO_2 nanocomposite particles at pH 7.45 and 7.20. Conditions: Particles, 0.01 g; Total volume, 30 mL; Temperature, 303 K; Contact time, 5 min.

The adsorption isotherm models are important for understanding interactive behavior and adsorption mechanism. The equilibrium isotherm models for adsorption of RN on

Preprints (www.preprints.org) | NOT PEER-REVIEWED | Posted: 11 July 2018 doi:10.20944/preprints201807.0205.v1

$Al_2O_3/Fe_3O_4/SiO_2$/PGMA nanocomposite particles are shown in Figures 8-10. The equilibrium data have been analyzed by linear regression of isotherm model equations and the related empirical constants obtained from the slope and intercept of the respective linear plot are displayed in Table 1. The data indicate that the Langmiur isotherm yielded the best fit, as supported by the highest correlation coefficient (R^2). This implies that homogeneous monolayer adsorption is preferably followed. The values of R_L are between 0 and 1, confirming the adsorption process as favorable. The theoretical maximum adsorption capacity q_{max} is maximum (69.44 mg g^{-1}) at 283K and decreases with increasing temperature. The value of K_f (Freundlich constant) also confirms that the adsorption of RN on nanocomposite particles is more favorable at lower temperature. Similarly the values of Temkin constant (B), which are related to the heat of adsorption of RN, decrease with increase in temperature and irrespective of temperature the value is lower than 8.0 Kj mol^{-1}. This indicates that the interaction between dye molecules and nanocomposite particle surface mostly followed physisorption [47]. Relatively low A_T values ascribe the low electrostatic interaction between RN dye and γ-$Al_2O_3/Fe_3O_4/SiO_2$/PGMA nanocomposite particles at different temperatures [48]. Physisorption is usually supported at lower temperature because at higher temperature the solubility and entropy of dye molecules are enhanced. The equilibrium adsorption isotherm models on γ-$Al_2O_3/Fe_3O_4/SiO_2$ nanocomposite particles are also analyzed (Figures S3-S5). The obtained equilibrium data and related empirical constants presented in Table 1 indicate that Langmuir isotherm is the best fit model. Hence the same monolayer surface coverage is preferably followed. The theoretical maximum adsorption capacity (q_{max}) of γ-$Al_2O_3/Fe_3O_4/SiO_2$ nanocomposite particles decreases from 129.87 to 121.95 mg g^{-1} with the increase of temperature from 283 K to 323 K. Therefore it can be said that adsorption of RN is favorable on both nanocomposite particles at lower temperature. The

Preprints (www.preprints.org) | NOT PEER-REVIEWED | Posted: 11 July 2018 doi:10.20944/preprints201807.0205.v1

theoretical maximum adsorption capacity of γ-Al_2O_3/Fe_3O_4/SiO_2/PGMA nanocomposite particles (1.30 mg m^{-2}) is relatively high compared to that of γ-Al_2O_3/Fe_3O_4/SiO_2 nanocomposite particles (0.87 mg m^{-2}). This result suggests that reactive epoxide functionality on γ-Al_2O_3/Fe_3O_4/SiO_2/PGMA nanocomposite particles acts as a driving force for the increase of adsorption capacity. The structure of RN is unknown due to commercial purpose but one can normally expect the presence of different types of functional groups such as S=O, –$CONH_2$/–CONH–, aromatic phenol and even may be primary or secondary amine. So there is enough chance to form hydrogen and/covalent bonds among ester-epoxide groups on the particle surface and reactive groups of RN dye molecules. Whereas the formation of such hydrogen and/covalent linkages with γ-Al_2O_3/Fe_3O_4/SiO_2 nanocomposite particles is scarcely possible.

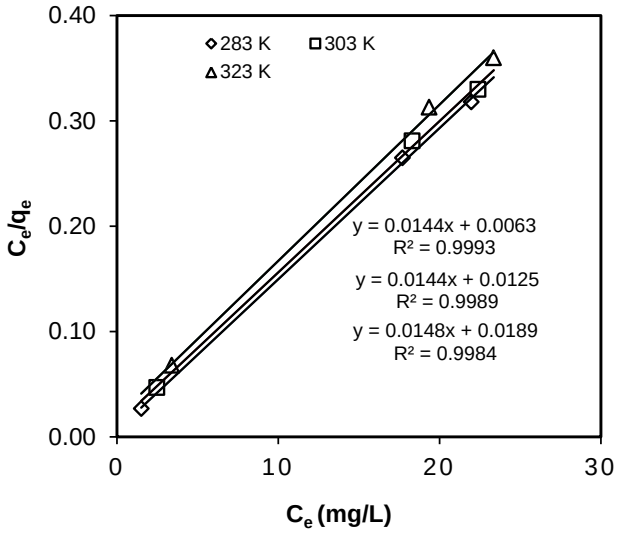

Figure 8. Langmuir isotherms for RN adsorption on γ-Al_2O_3/Fe_3O_4/SiO_2/PGMA nanocomposite particles. Conditions: Particles, 0.01 g; Total volume, 30 mL; pH, 7.45; Contact time, 5 min.

Preprints (www.preprints.org) | NOT PEER-REVIEWED | Posted: 11 July 2018 doi:10.20944/preprints201807.0205.v1

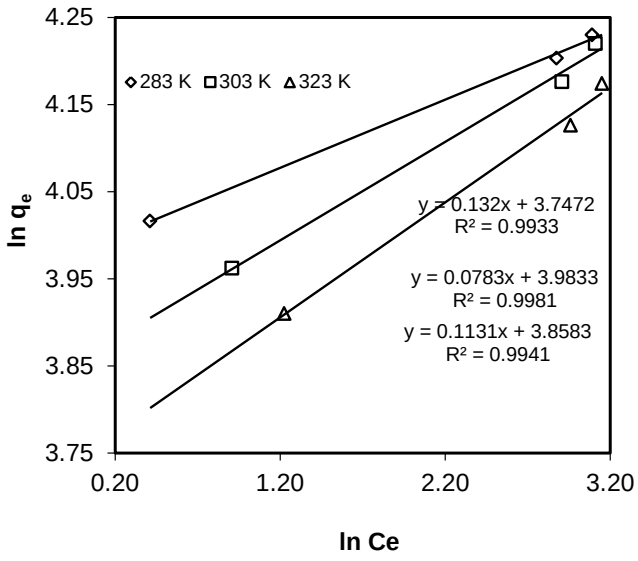

Figure 9. Freundlich isotherms for RN adsorption on γ-Al_2O_3/Fe_3O_4/SiO_2/PGMA nanocomposite particles. Conditions: Particles, 0.01 g; Total volume, 30 mL; pH, 7.45; Contact time, 5 min.

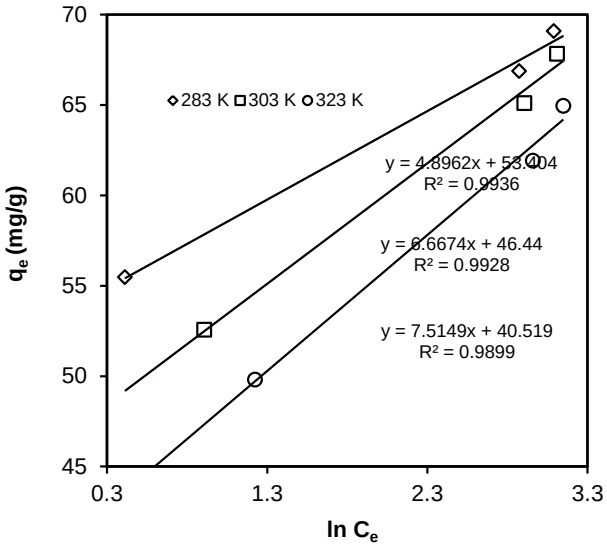

Figure 10. Temkin isotherms for RN adsorption on γ-Al_2O_3/Fe_3O_4/SiO_2/PGMA nanocomposite particles. Conditions: Particles, 0.01 g; Total volume, 30 mL; pH, 7.45; Contact time, 5 min.

Preprints (www.preprints.org) | NOT PEER-REVIEWED | Posted: 11 July 2018 doi:10.20944/preprints201807.0205.v1

Table 1. Empirical constants for the adsorption of RN on nanocomposite particles**.**

γ-Al_2O_3/Fe_3O_4/SiO_2/PGMA												
T (K)	Langmuir constants					Freundlich constants				Temkin constants		
	q_{max} (mg/g)	q_{max} (mg/m^2)	b (L/mg)	R^2	R_L	n	K_f (mg/g)	K_f (mg/m^2)	R^2	A_T (L/mg)	B (J/mol)	R^2
283	69.44	1.306	2.272	0.9993	0.01	12.77	53.69	1.001	0.9981	1.12	480.49	0.9936
303	69.44	1.306	1.15	0.9989	0.019	8.84	47.38	0.891	0.9941	1.13	377.83	0.9928
323	67.57	1.270	0.783	0.9984	0.0276	7.57	42.40	0.797	0.9933	1.12	357.35	0.9899
γ-Al_2O_3/Fe_3O_4/SiO_2												
283	129.87	0.867	1.35	0.9980	0.0122	16.37	104.19	0.696	0.7895	1.371	327.382	0.7713
303	125.00	0.835	0.96	0.9985	0.0171	11.67	91.90	0.614	0.939	1.40	269.37	0.9176
323	121.95	0.815	0.68	0.9969	0.024	9.840	83.34	0.556	0.8942	1.38	251.703	0.8693

Thermodynamic equilibrium constant, K_c, calculated from intercept of the plots of ln (q_e/C_e) against q_e (Figure S6), decreases with increasing temperature irrespective of nanocomposite particles (Table 2). Thermodynamic parameters ΔH and ΔS were calculated from the slope and intercept of the linear plot of ln K_C against $1/T$ (Figure S7) using Van't Hoff equation (eq. 6) and subsequently ΔG values were obtained from eq. 7. Irrespective of temperature ΔG values are negative and lie in the range $-20 < \Delta G < 0$ kJ/mol. This indicates that the adsorption process is physical and thermodynamically favorable [47]. The more negative value of ΔG at lower temperature again supports that adsorption is preferable at lower temperature. The negative value of ΔH suggests the adsorption process as exothermic. Comparatively the more negative value of ΔS for adsorption on γ-Al_2O_3/Fe_3O_4/SiO_2/PGMA nanocomposite particles indicates that adsorbed dye molecules are less disordered at the interface [49,50]. This perhaps indicates the formation of physical as well as chemical bonding (preferably hydrogen bonding) between RN and epoxide functionality on γ-Al_2O_3/Fe_3O_4/SiO_2/PGMA nanocomposite particles.

Preprints (www.preprints.org) | NOT PEER-REVIEWED | Posted: 11 July 2018 doi:10.20944/preprints201807.0205.v1

Table 2. Thermodynamic parameters for the adsorption of RN on nanocomposite particles.

γ-Al_2O_3/Fe_3O_4/SiO_2/PGMA			
Thermodynamic constant	**Temperature (K)**		
	283 K	303 K	323K
K_c	13.934	9.9501	8.3392
ΔG° (kJ / mol)	-6.22	-5.91	-5.61
ΔH° (kJ / mol)	-10.60		
ΔS° (J mol^{-1} K^{-1})	-15.46		
γ-Al_2O_3/Fe_3O_4/SiO_2			
K_c	14.377	12.695	10.014
ΔG° (kJ / mol)	-6.40	-6.30	-6.21
ΔH° (kJ / mol)	-7.69		
ΔS° (J mol^{-1} K^{-1})	-4.57		

Kinetics of adsorption data was analyzed at 303 K using kinetic models to determine the rate expression. Pseudo-first-order model was not used as the value of R^2 obtained from the plot of ln (q_e - q_t) versus t was less than 0.50. The pseudo-second-order (P-S-O) model was therefore used to investigate the kinetics of the adsorption of RN dye on nanocomposite particles. The equation of the P-S-O kinetic model is as follows:

$t/q_t = 1/K_2 q^2_e + (1/q_e) t$ ---------- (8)

where K_2 is the equilibrium rate constant of the P-S-O adsorption (g mg^{-1} min^{-1}), q_e is the maximum adsorption capacity (mg g^{-1}) for the P-S-O adsorption, and q_t is the adsorption capacity (mg g^{-1}) at any adsorption time t (min). For γ-Al_2O_3/Fe_3O_4/SiO_2/PGMA nanocomposite particles the obtained value of R^2 (0.9996) from the plot of t/q_t against t (Figure 11) shows that this kinetic model is applicable to describe the adsorption kinetics and the experimental q_{max} (88.08 mg g^{-1}) is consistent with the calculated q_e (87.72 mg g^{-1}) value. Similarly for γ-Al_2O_3/Fe_3O_4/SiO_2 nanocomposite particles P-S-O kinetic model (Figure S8) is applicable as the value of R^2 is close to unity (0.9966) and the experimental q_{max} (141.33 mg g^{-1}) is close to the theoretical value of q_e (142.86 mg g^{-1}).

Preprints (www.preprints.org) | NOT PEER-REVIEWED | Posted: 11 July 2018 doi:10.20944/preprints201807.0205.v1

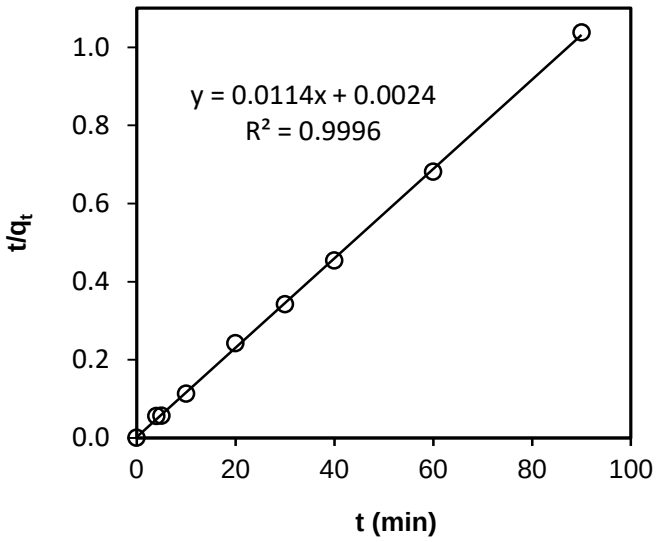

Figure 11. Pseudo second order model for adsorption of RN on γ-Al_2O_3/Fe_3O_4/SiO_2/PGMA nanocomposite particles.

Regeneration and reuse of adsorbent materials are crucial from the view point of industrial application, process economy and preventing pollution from used adsorbent. The adsorption-desorption-reuse cycles were carried out three times and the results are displayed in Figure 12. Treatment of dye loaded γ-Al_2O_3/Fe_3O_4/SiO_2/PGMA nanocomposite particles with 1M NaOH solution did not decrease the adsorption magnitude of RN in the third cycle as the recovered particles retained almost 99% adsorption efficiency. Hence it can be said that γ-Al_2O_3/Fe_3O_4/SiO_2/PGMA nanocomposite particles can be used as adsorbent for the removal of dye from contaminated water coming out from dyeing industry. It is worthwhile to mention that γ-Al_2O_3/Fe_3O_4/SiO_2 nanocomposite particles also had the same adsorption efficiency in the third cycle (data not shown).

Preprints (www.preprints.org) | NOT PEER-REVIEWED | Posted: 11 July 2018 doi:10.20944/preprints201807.0205.v1

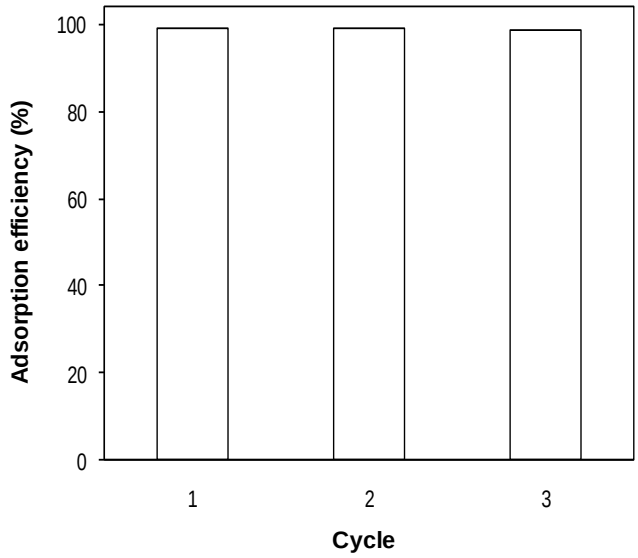

Figure 12. Relationship between reuse cycle and the percent adsorption efficiency of RN dye molecules by γ-Al_2O_3/Fe_3O_4/SiO_2/PGMA nanocomposite particles. Conditions: RN, 50 mg L^{-1}; Particles, 0.035 g; Total volume, 30 mL; Temperature, 303 K; Contact time, 5 min.

The interaction of RN with γ-Al_2O_3/Fe_3O_4/SiO_2/PGMA nanocomposite particles was evaluated by recording FTIR spectra of the adsorbent materials before and after adsorption. In the FTIR spectrum of RN dye (Figure S9) the broad signal at 3438 cm^{-1} represents –NH stretching vibration, sharp signal at 1611 cm^{-1} represents N=N stretching vibration of azo compounds, signal at 1481 cm^{-1} represents N−H trans stretching of secondary amides, signal at 1130 cm^{-1} corresponds to S=O asymmetric stretching of sulfones and signals at 720 and 618 cm^{-1} correspond to C–H bending vibrations. The spectrum of γ-Al_2O_3/Fe_3O_4/SiO_2/PGMA nanocomposite polymer particles before dye adsorption shows strong absorption signals at 1729.10 and 1153.40 cm^{-1} for C=O and C–O stretching vibrations of ester group, weak absorption bands at around 958 and 848 cm^{-1} represent epoxide group, absorption signal at 2930 cm^{-1} due to aliphatic signal for C-H stretching vibration and bands at 1630 and 3435 cm^{-1}

Preprints (www.preprints.org) | NOT PEER-REVIEWED | Posted: 11 July 2018 doi:10.20944/preprints201807.0205.v1

represent the H–O–H stretching and bending vibrations. Comparatively after RN adsorption the signal intensities of C=O and C–O stretching vibrations of ester group are suppressed. N−H trans stretching signal of secondary amides in dye molecules is not visible in the dye loaded nanocomposite particles. Weak signals due to C–H bending vibrations of dye molecules are visible in the spectrum of nanocomposite particles after dye adsorption. The signals due to epoxide group of GMA could not be resolved because some unidentified signals are also present in dye molecules in the same region. The change in environment around ester group of nanocomposite particles and secondary amide group of dye molecules at least suggests the formation of hydrogen bonding between dye molecules and nanocomposite particles. The epoxide group is also expected to participate in such bonding with amide group of dye molecules but it could not be confirmed from the existing spectra due to overlapping signals from dye molecules in the same region.

4. Conclusion

Flake shaped and porous γ-Al_2O_3 particles prepared by sol-gel technique were doped with magnetic iron oxide nanoparticles. The magnetic nanocomposite particles were then modified with mesoporous SiO_2 layer and finally with PGMA layer via seeded polymerization. The introduction of epoxide PGMA layer slightly reduced the magnetic property but still they were strongly paramagnetic and moved under the external magnetic field. The surface activity of γ-Al_2O_3/Fe_3O_4/SiO_2/PGMA nanocomposite particles was studied by measuring the adsorption behavior of RN a reactive azo dye and the results were compared with those of γ-Al_2O_3/Fe_3O_4/SiO_2 as reference materials. The adsorption rate was very fast and reached equilibrium in 5 min. The amount of adsorption was dependent on the initial concentration of RN

Preprints (www.preprints.org) | NOT PEER-REVIEWED | Posted: 11 July 2018 doi:10.20944/preprints201807.0205.v1

and adsorption was favorable at lower temperature (283 K). Irrespective of the nature of nanocomposite particles the correlation coefficients (R^2) of Langmuir, Freundlich and Temkin confirmed that adsorption process at any temperature could be best explained by Langmuir isotherm. The introduction of epoxide functionality increased the maximum theoretical adsorption capacity per unit surface area from 0.87 mg m^{-2} in γ-Al_2O_3/Fe_3O_4/SiO_2 nanocomposite particles to 1.30 mg m^{-2} in γ-Al_2O_3/Fe_3O_4/SiO_2/PGMA nanocomposite particles. The increased adsorption capacity of γ-Al_2O_3/Fe_3O_4/SiO_2/PGMA nanocomposite particles was speculated to be due to the formation of hydrogen bonding in addition to Van der Waals interaction with dye molecules. The possibility of the formation covalent linkage is also there provided RN dye molecules contained reactive amine groups as most of the reactive azo dyes. The negative value of ΔG and ΔH (-10.60 kJ/mol) suggested that the adsorption process was spontaneous and exothermic in nature. A comparison between experimental and theoretical adsorption capacities suggested that kinetic data can be described by the pseudo-second-order equation.

Acknowledgments: Financial support from MOST, Dhaka (Econ. Code: 3-2601-3993-5901) is gratefully acknowledged. Authors also acknowledged Central Science Laboratory, Rajshahi University for instrument support.

Author Contributions: S.S.B. performed the experiments; M. Mostafizar Rahman, M. Mahbubor Rahman, M.A.A. and M.R.K. analyzed the data; H.A. conceived and designed the research idea. S.S.B and H.A. contributed in preparing the manuscript.

Conflicts of Interest: The authors declare no conflict of interest.

Preprints (www.preprints.org) | NOT PEER-REVIEWED | Posted: 11 July 2018 doi:10.20944/preprints201807.0205.v1

Appendix A. Supplementary data

Supplementary data associated with this article can be found in the online version.

References

1. Li, S.; Shi, Y.; Cai, N. Potassium-promoted γ-alumina adsorbent from K_2CO_3 coagulated alumina sol for warm gas carbon dioxide separation. *ACS Sustainable Chem. Eng*. **2015**, *3*, 111−116.
2. Yanagishita, T.; Fujimura, R.; Nishio, K.; Masuda, H. Fabrication of monodisperse polymer nanoparticles by membrane emulsification using ordered anodic porous alumina. *Langmuir* **2010**, *26*, 1516–1519.
3. Asencios, Y.J.O.; Sun-Kou, M.R. Synthesis of high-surface-area γ-Al_2O_3 from aluminum scrap and its use for the adsorption of metals: Pb(II), Cd(II) and Zn(II). *Appl. Surface Sci.* **2012**, *258*, 10002-10011.
4. Shan, G.B.; Chen, Y.Z.; Gong, M.M.; Dong, H.; Li, B.; Liu, F. Influence of Al_2O_3 particle pinning on thermal stability of nanocrystalline Fe. *J. Mater. Sci. Technol.* **2018**, *34*, 599-604.
5. Liu, Y.; Gonçalves, A.A.S.; Zhou, Y.; Jaroniec, M. Importance of surface modification of c-alumina in creating its nanostructured composites with zeolitic imidazolate framework ZIF-67. *J. Colloid Interface Sci*. **2018**, *526*, 497–504.
6. Wang, G.; Zhang, K. Superplastic properties of Al_2O_3/Ni-Mn nanocomposite fabricated by electrodeposition. *J. Mater. Sci. Technol*. **2010**, *26*, 625-628.

Preprints (www.preprints.org) | NOT PEER-REVIEWED | Posted: 11 July 2018 doi:10.20944/preprints201807.0205.v1

7. Khabibullin, A.; Bhangaonkar, K.; Mahoney, C.; Lu, Z.; Schmitt, M.; Sekizkardes, K.A.; Bockstaller, M.R.; Matyjaszewski, K. Grafting PMMA brushes from α-alumina nanoparticles via SI-ATRP. *ACS Appl. Mater. Interfaces* **2016**, *8*, 5458−5465.

8. Popat, K.C.; Mor, G.; Grimes, C.A.; Desai, T.A. Surface modification of nanoporous alumina surfaces with poly(ethylene glycol). *Langmuir* **2004**, *20*, 8035-8041.

9. Jackson, B.R.; Liu, X.; McCandlish, E.F.; Riman, R.E. Self-assembly of monolayer-thick alumina particle−epoxy composite films. *Langmuir* **2007**, *23*, 11399-11403.

10. Cho, G.; Glatzhofer, D.T.; Fung, B.M.; Yuan, W.–L.; O'Rear, E.A. Formation of ultrathin polypyrrole (PPY) films on alumina particles using adsorbed hexanoic acid as a template. *Langmuir* **2000**, *16*, 4424-4429.

11. Anaya, S.; Serrano, B.; Herrero, B.; Cervera, A.; Baselga, J. γ‑Alumina modification with long chain carboxylic acid surface nanocrystals for biocompatible polysulfone nanocomposites. *ACS Appl. Mater. Interfaces* **2014**, *6*, 14460-14468.

12. Dong, Z.; Wu, Y.; Wang, Q.; Xie, C.; Ren, Y.; Clark, R.L. Reinforcement of electrospun membranes using nanoscale Al_2O_3 whiskers for improved tissue scaffolds. *J. Biomed. Mater. Res. Part A* **2012**, *100A*, 903-910.

13. Sánchez-Valente, J.; Hernández, F. Physicochemical and catalytic properties of sol−gel aluminas aged under hydrothermal conditions. *Langmuir* **2003**, *19*, 3583-3588.

14. Nassar, N.N.; Hassan, A.; Pereira-Almao, P. Effect of the particle size on asphaltene adsorption and catalytic oxidation onto alumina particles. Energy Fuels **2011**, *25*, 3961-3965.

15. Lei, Z.; Zhao, K.; Wang, Y.; An, L. Thermal expansion of Al matrix composites reinforced with hybrid micro-/nano-sized Al_2O_3 particles. *J. Mater. Sci. Technol*. **2014**, *30*, 61-64.

Preprints (www.preprints.org) | NOT PEER-REVIEWED | Posted: 11 July 2018 doi:10.20944/preprints201807.0205.v1

16. Ghasemi, M.; Dehkordi, A.M. Transesterification of waste cooking oil to biodiesel using KOH/γ-Al_2O_3 catalyst in a new two-impinging-jets reactor. *Ind. Eng. Chem. Res*. **2014**, *53*, 12238-12248.

17. Bristy, S.S.; Rahman, M.A.; Tauer, K.; Minami, H.; Ahmad, H. Preparation and characterization of magnetic γ-Al_2O_3 ceramic nanocomposite particles with variable Fe_3O_4 content and modification with epoxide functional polymer. *Ceramic Int*. **2018**, *44*, 3951-3959.

18. Chen, B.Y.; Zhang, M.M.; Chang, C.T.; Ding, Y.; Lin, K.I.; Chiou, C.S.; Hseuh, C.C.; Xu, H. Assessment upon azo dye decolorization and bioelectricity generation by *Proteus hauseri*. *Bioresour. Technol*. **2010**, *101*, 4737-4741.

19. Jadhav, J.P.; Phugar, S.S.; Dhanve, R.S.; Jadhav, S.B. Rapid biodegradation and decolorization of Direct Orange 39 (Orange TGLL) by an isolated bacterium *Pseudomonas aeruginosa* strain BCH. *Biodegradation* **2010**, *22*, 453-463.

20. Golka, K.; Kopps, S.; Myslak, Z.W. Carcinogenicity of azo colorants: influence of solubility and bioavailability. *Toxicol. Lett*. **2004**, *151*, 203–210.

21. Ahmad, H.; Nurunnabi, M.; Rahman, M.M.; Kumar, K.; Tauer, K.; Minami, H.; Gafur, M.A. Magnetically doped multi stimuli-responsive hydrogel microspheres with IPN structure and application in dye removal. *Colloids and Surfaces A: Physicochem. Eng. Aspects* **2014**, *459*, 39-47.

22. Huang, X.; Zhan, X.; Wen, C.; Xu, F.; Luo, L. Amino-functionalized magnetic bacterial cellulose/activated carbon composite for Pb^{2+} and methyl orange sorption from aqueous solution. *J. Mater. Sci. Technol*. **2018**, *34*, 855-863.

Preprints (www.preprints.org) | NOT PEER-REVIEWED | Posted: 11 July 2018 doi:10.20944/preprints201807.0205.v1

23. Molavi, H.; Hakimian, A.; Shojaei, A.; Raeiszadeh, M. Selective dye adsorption by highly water stable metal-organic framework: long term stability analysis in aqueous media. *Appl. Surf. Sci.* **2018**, *445*, 425-436.

24. Jian, S.; Wang, S.; Tan, Y. Preparation of lysine-decorated polymer-brush-grafted magnetic nanocomposite for the efficient and selective adsorption of organic dye. *Appl. Surf. Sci*. **2018**, *441*, 654-662.

25. Horák, D.; Trchová, M.; Beneš, M.J.; Veverka, M.; Pollert, E. Monodisperse magnetic composite poly(glycidyl methacrylate)/$La_{0.75}Sr_{0.25}MnO_3$ microspheres by the dispersion polymerization. *Polymer* **2010**, *51*, 3116-3122.

26. Alam, M.A.; Rabbi, M.A.; Miah, M.A.J.; Rahman, M.M.; Rahman, M.A.; Ahmad, H. A versatile approach on the preparation of dye-labeled stimuli-responsive composite polymer particles by surface modification. *J. Colloid Sci. Biotechnol*. **2012**, *1*, 225-234.

27. Khan, B.A.; Na, H.; Chevali, V.; Warner, P.; Zhu, J.; Wang, H. Glycidyl methacrylate-compatibilized poly(lactic acid)/hemp hurd biocomposites: processing, crystallization, and thermo-mechanical response. *J. Mater. Sci. Technol.* **2018**, *34*, 387-397.

28. Cardoso, N.F.; Pinto, R.B.; Lima, E.C.; Calvete, T.; Amavisca, C.V.; Royer, B.; Cunha, M.L.; Fernandes, T.H.M.; Pinto, I.S. Removal of remazol black B textile dye from aqueous solution by adsorption. *Desalination* **2011**, *269*, 92-103.

29. Mafra, M.R.; Igarashi-Mafra, L.; Zuim, D.R.; Vasques, E.C.; Ferreira, M.A. Adsorption of remazol brilliant blue on an orange peel adsorbent. *Braz. J. Chem. Eng*. **2013**, *30*, 657-665.

30. Sun, D.; Zhang, Z.; Wang, M.; Wu, Y. Adsorption of reactive dyes on activated carbon developed from Enteromorpha prolifera. *Am. J. Analytical Chem*. 2013, 4, 17-26.

Preprints (www.preprints.org) | NOT PEER-REVIEWED | Posted: 11 July 2018 doi:10.20944/preprints201807.0205.v1

31. Chen, Y.; Zhang, H.; Cai, X.; Ji, J.; He, S.; Zhai, G. Multifunctional mesoporous silica nanocarriers for stimuli-responsive target delivery of anticancer drugs. *RSC Adv*. **2016,** *6*, 92073-92091.

32. Sponchia, G.; Marin, R.; Freris, I.; Marchiori, M.; Moretti, E.; Storaro, L.; Canton, P.; Lausi, A.; Benedetti, A.; Riello, P. Mesoporous silica nanoparticles with tunable pore size for tailored gold nanoparticles. *J. Nanopart. Res*. **2014**, *16*, ID 2245.

33. Langmuir, I. The constitution and fundamental properties of solids and liquids. Part I. Solids. *J. Am. Chem. Soc*. **1961**, *38*, 2221-2295.

34. Freundlich, H.M.F. Over the adsorption in solution. *J. Phys. Chem*. **1906**, *57*, 385-471.

35. Temkin, M.I. Adsorption equilibrium and the kinetics of processes on nonhomogeneous surfaces and in the interaction between adsorbed molecules. *Zh. Fiz. Chim*. **1941**, *15*, 296-332.

36. Lee, T.; Park, S.S.; Jung, Y.; Ha, C.-S. Preparation and characterization of polyimide/mesoporous silica hybrid nanocomposites based on water-soluble poly(amic acid) ammonium salt. *Eur. Polym. J*. **2009**, *45*, 19-29.

37. Aks, Z.; Tezer, S. Equilibrium and kinetic modelling of biosorption of Remazol Black B by *Rhizopus arrhizus* in a batch system: effect of temperature. *Process Biochem*. **2000,** *36*, 431-439.

38. Alves de Lima, R.O.; Bazo, A.P.; Salvadori, D.M.F.; Rech, C.M.; Oliveira, D.D.P.; Umbuzeiro, G.A. Mutagenic and carcinogenic potential of a textile azo dye processing plant effluent that impacts a drinking water source. *Mutat. Res*. **2007**, *626*, 53-60.

Preprints (www.preprints.org) | NOT PEER-REVIEWED | Posted: 11 July 2018 doi:10.20944/preprints201807.0205.v1

39. Birhanl, A.; Ozmen, M. Evaluation of the toxicity and teratogenity of six commercial textile dyes using the frog embryo teratogenesis assay-Xenopus. *Drug Chem. Toxicol*. **2005**, *28*, 51-65.

40. Silva, M.C.; Torres, J.A.; de Sá, V.; Chagas, L.R.P.M.B.; Ferreira-Leitão, V.S.; Correâ, A.D. The use of soybean peroxidase in the decolourization of Remazol Brilliant Blue R and toxicological evaluation of its degradation products. *J. Mol. Catal. B: Enzym*. **2013**, *89*, 122-129.

41. Jadhav, S.B.; Phugare, S.S.; Patil, P.S.; Jadhav, J.P.; Biochemical degradation pathway of textile dye Remazol red and subsequent toxicological evaluation by cytotoxicity, genotoxicity and oxidative stress studies. *Int. Biodeterior. Biodegrad*. **2011**, *65*, 733-743.

42. Jain, A.K.; Gupta, V.K.; Bhatnagar, A.; Jain, S.; Suhas, S. A comparative assessment of adsorbents prepared from industrial wastes for the removal of cationic dye. *J. Ind. Chem. Soc*. **2003**, *80*, 267-270.

43. Bharathi, K.S.; Ramesh, S.T. Removal of dyes using agricultural waste as low-cost adsorbents: a review. *Appl. Water Sci*. **2013**, *3*, 773-790.

44. Çelekli, A.; Birecikligil, S.S.; Geyik, F.; Bozkurt, H. Prediction of removal efficiency of Lanaset Red G on walnut husk using artificial neural network model. *Bioresour. Technol*. **2012**, *103*, 64-70.

45. Venkatesha, T.G.; Viswanatha, R.; Nayaka, Y.A.; Chethana, B.K. Kinetics and thermodynamics of reactive and vat dyes adsorption on MgO nanoparticles. *Chem. Eng. J*. **2012**, *198-199*, 1-10.

Preprints (www.preprints.org) | NOT PEER-REVIEWED | Posted: 11 July 2018 doi:10.20944/preprints201807.0205.v1

46. Khairy, M.; Kamal, R.; Amin, N.H.; Mousa, M.A. Kinetics and isotherm studies of Remazol Red adsorption onto polyaniline/cerium oxide nanocomposites. *J. Basic Environ. Sci.* **2016**, *3*, 123-132.

47. Jalil, A.A.; Triwahyono, S.; Yaakob, M.R.; Azmi, Z.Z.A.; Sapawe, N.; Kamarudin, N.H.N.; Setiabudi, H.D.; Jaafar, N.F.; Sidik, S.M.; Adam, S.H.; Hameed, B.H. Utilization of bivalve shell-treated *Zea mays* L. (maize) husk leaf as a low-cost biosorbent for enhanced adsorption of malachite green. *Bioresour. Technol*. **2012**, *120*, 218-224.

48. Sun, P.; Hui, C.; Khan, R.A.; Du, J.; Zhang, Q.; Zhao, Y.–H. Efficient removal of crystal violet using Fe_3O_4-coated biochar: the role of the Fe_3O_4 nanoparticles and modeling study their adsorption behavior. *Scientific Reports* **2015**, *5*, ID12638.

49. Ho, Y.S.; Ng, J.C.Y.; Mckay, G. Kinetics of pollutant sorption by biosorbents: Review. *Sep. Purif. Method* **2000**, *29*, 189-191.

50. Chen, G.-C.; Shan, X.-Q.; Zhou, Y.-Q.; Shen, X.; Huang, H.-L.; Khan, S.U. Adsorption kinetics, isotherms and thermodynamics of atrazine on surface oxidized multiwalled carbon nanotubes. *J. Hazard. Mater*. **2009**, *169*, 912-918.